A Comparison of the Bounded Derivative and the Normal-Mode Initialization Methods Using Real Data

F. H. M. SEMAZZI* AND I. M. NAVON**

Laboratory for Atmospheres, NASA/Goddard Space Flight Center, Greenbelt, MD 20771

(Manuscript received 15 July 1985, in final form 17 April 1986)

ABSTRACT

Application of the bounded-derivative and normal-mode methods to a simple linear barotropic model at a typical middle latitude shows that the two methods lead to identical constraints up to a certain degree of approximation. Beyond this accuracy the two methods may differ from each other.

When applied to a global nonlinear barotropic model using real data, again the two methods lead to similar balanced initial states. The gravity oscillations in the unbalanced height field, which have amplitudes of up to 60 m with a dominant periodicity of about 5 to 6 h, are practically eliminated by both initialization methods. The rotational wind component is smooth even for the unbalanced initial state. The small-scale spatial features of the irrotational wind component are drastically reduced by initialization. Both the nonlinear normal-mode and the bounded-derivative initialization methods yield similar divergence fields centered around the areas of highest orography.

The comparison shows that there is no significant loss of information in the mass and momentum fields, despite the fact that the bounded-derivative method employs only the original, rotational wind component to construct a balanced initial state compared to the normal-mode method, which, in addition, makes use of the unbalanced divergent wind and height fields.

1. Introduction

In the field of numerical weather prediction, it is desirable to use the primitive equations, which are the Eulerian or Lagrangian hydrodynamical equations modified by the assumption of hydrostatic balance. These equations govern two types of motion. One is low-frequency motion, which is responsible for weather patterns generally observed on synoptic weather charts. The second category belongs to high-frequency, gravity inertia motions, which in the real atmosphere play a secondary role.

Regarding numerical models, unwanted gravitational waves are superimposed on the low-frequency motions, which are meteorologically significant. Therefore, it is desirable to eliminate or effectively suppress the generation of these motions. There are two relatively new methods that have been developed to specify appropriate balance concerning initial data in order to control the excitation of gravitational motions, namely, the normal-mode (NMI) and bounded-derivative (BDI) initialization methods.

The NMI method has been used extensively since it was introduced independently by Baer (1977) and Machenhauer (1977). This method requires the construction of free normal modes where frequency is determined as the eigenvalue. The existence of a separation gap in frequency between gravitational and meteorological modes allows construction of a balanced initial state free of high-frequency motion tendencies. Earlier application of the NMI method encountered many severe problems (Daley, 1981). Recently, however, considerable progress has been made in understanding some of these difficulties. For instance, Puri (1985) has unveiled some of the reasons for the difficulties experienced when diabatic heating is included in the NMI process. New advances have also been made regarding some long-standing convergence problems associated with Machenhauer's iteration scheme (Kitade, 1983; Rasch, 1985). Tribbia (1984) has proposed a new approach for obtaining higher-order corrections to Machenhauer's scheme. In this method, the projection of the nonlinear forcing on the gravitational manifold is expanded in Taylor series around the initial time. The result is a generalized iteration equation where the first term corresponds to the standard, nonlinear, normal-mode initialization. A more refined initial balance can be obtained to any order by incorporating higher-order terms in the expansion. The prospect of extending the application of NMI to limited area domains has also attracted much attention. For instance, Briere (1982) and Bourke and McGregor (1983) have presented encouraging results in this regard, but considerable difficulties have yet to be resolved.

* Present affiliation: Department of Meteorology, University of Maryland, College Park, MD 20742.

** Present affiliation: Supercomputer Computations Research Institute, Florida State University, Tallahassee, FL 32306.

© 1986 American Meteorological Society

Recently, Kreiss (1979, 1980) gave a general theory of filtering motions of unwanted time scales by bounding the time derivatives of symmetric hyperbolic systems similar in form to equations for atmospheric motion and plasma physics. To apply the bounded-derivative method, the first step is to define the characteristic scales of motion of primary interest. The terms that contribute to large time derivatives are identified through scale analysis of the dynamical equations. These terms are constrained to ensure that the time derivatives are on the order of the slow time scale. The larger the number of higher-order time derivatives for which this condition is satisfied, the smoother is the time evolution of the solution. Browning et al. (1980) introduced the application of the bounded-derivative initialization method to numerical weather prediction to obtain balanced data for a barotropic model, including the effect of orography. Browning (1982) addressed the problem of extending the application of the bounded derivative method to domains with open boundaries. In another important study, Kasahara (1982) theoretically investigated the connection between the BDI and NMI and showed that the two methods are equivalent within a certain degree of approximation. A priori, it is not clear whether the same degree of agreement will prevail when real data are used. Moreover, the BDI has not really been tested using realistic initial data.

The purposes of this study are the extension of the application of the BDI method to real data and the comparison of the results with NMI. In section 2 we briefly review some concepts regarding the BDI and NMI methods using a simple linear model. A nonlinear global barotropic model is introduced in section 3. The BDI and NMI schemes for the model in section 3 are described in section 4. The comparison of BDI and NMI is discussed in section 5 for the fourth-order GLA (Goddard Laboratory for Atmospheres) global barotropic model and concluding remarks are presented in section 6.

2. Linear model

Before discussing the results arising from the nonlinear model experiments, it is useful as a reference to examine some implications of a simple or linearized one-level model in x, t coordinates. In this section we first rescale this model and then use the BDI method to obtain the relevant constraints that the initial data must certify in order to yield a smooth forecast. We also independently derive initial constraints following the NMI method and compare them with the BDI constraints. Lastly, forecasts based on the linear model are performed to examine the impact of various initial conditions, including the ones based on the BDI and NMI methods. Linearization is performed about a basic state, which consists of a uniform zonal current $\bar{U}$ and geostrophically balanced height $\bar{h}$. We express the linearized system in the form

$$\left.\begin{aligned} u_t + gh_x - fv &= -\bar{U}u_x \\ v_t + fu &= -\bar{U}v_x \\ h_t + \bar{h}u_x &= \bar{U}(fv/g - h_x) \end{aligned}\right\}, \tag{2.1}$$

where x is the Cartesian coordinate directed westward; t is time; u, v and h are deviations of zonal velocity, meridional velocity and height, respectively, from the basic state. As usual, g is the acceleration due to gravity of the earth and f is the Coriolis parameter. It is convenient to assume harmonic dependence and assume that

$$\begin{pmatrix} u \\ v \\ h \end{pmatrix} = \begin{pmatrix} \tilde{u} \\ \tilde{v} \\ \tilde{h} \end{pmatrix} \exp[ikx], \tag{2.2}$$

where $\tilde{u}$, $\tilde{v}$, and $\tilde{h}$ are functions of time only. Also, i is the unit complex number and k is the wavenumber. Substituting (2.2) into (2.1) yields a pure initial value problem of the form

$$\left.\begin{aligned} \tilde{u}_t + ik\bar{U}\tilde{u} + igk\tilde{h} - f\tilde{v} &= 0 \\ \tilde{v}_t + ik\bar{U}\tilde{v} + f\tilde{u} &= 0 \\ \tilde{h}_t + ik\bar{U}\tilde{h} - \bar{U}f\tilde{v}/g + ik\bar{h}\tilde{u} &= 0 \end{aligned}\right\}. \tag{2.3}$$

Next, we scale (2.3) and assume that the characteristic scales of a typical, middle-latitude synoptic disturbance are

$$\left.\begin{aligned} &L && \text{horizontal scale} \approx 10^6\,\text{m} \\ &\tilde{H} && \text{height perturbation} \approx 10^2\,\text{m} \\ &\bar{H} && \text{height mean} \approx 10^4\,\text{m} \\ &\tilde{V} && \text{horizontal particle speed} \approx 10\,\text{m s}^{-1} \\ &T && (=L/\tilde{V}) = 10^5\,\text{s} \\ &K && \text{characteristic wavenumber} \approx 10^{-6}\,\text{m}^{-1} \\ &G && \text{gravity acceleration} \approx 10\,\text{m s}^{-2} \\ &F && \text{Coriolis parameter} = 10^{-4}\,\text{s}^{-1} \end{aligned}\right\}. \tag{2.4}$$

By introducing the prime notation to identify the scaled quantities that are of order unity we write

$$\left.\begin{aligned} \tilde{u}' &= \tilde{u}/\tilde{V}, & x' &= x/L \\ \tilde{v}' &= \tilde{v}/\tilde{V}, & k' &= k/K \\ \tilde{h}' &= \tilde{h}/\tilde{H}, & g' &= g/G \\ t' &= t/T, & \bar{U}' &= \bar{U}/\tilde{V} \\ \bar{h}' &= \bar{h}/\bar{H}, & f' &= f/F \end{aligned}\right\}. \tag{2.5}$$

Substitution of (2.5) into (2.3) leads to the scaled system of equations. Dropping the primes for simplicity but remembering that all quantites are of order unity except the scaling parameter, $\epsilon = O(10^{-1})$, we find that

$$\left.\begin{aligned}\tilde{u}_t + ik\bar{U}\tilde{u} + \epsilon^{-1}(igk\tilde{h} - f\tilde{v}) = 0\\ \tilde{v}_t + ik\bar{U}\tilde{v} + \epsilon^{-1}f\tilde{u} = 0\\ \tilde{h}_t + ik\bar{U}\tilde{h} - \bar{U}f\tilde{v}/g + \epsilon^{-2}ik\bar{h}\tilde{u} = 0\end{aligned}\right\}. \quad (2.6)$$

To ensure that u_t, v_t and h_t are on the order of the slow time scale, i.e., O(1), we follow Browning et al. (1980) and express the first-order constraints as

$$\left.\begin{aligned}igk\tilde{h} - f\tilde{v} = \epsilon a\\ f\tilde{u} = \epsilon b\\ ik\bar{h}\tilde{u} = \epsilon^2 c\end{aligned}\right\}, \quad (2.7)$$

where a, b and c are smooth and of order unity. The simplest way to satisfy these conditions is to assume $a = b = c = 0$ at $t = 0$, in which case (2.7) leads to

$$\left.\begin{aligned}\frac{\tilde{v}}{\tilde{h}} = igk/f\\ \frac{\tilde{u}}{\tilde{h}} = 0\end{aligned}\right\}. \quad (2.8)$$

The constraints described by (2.8) are identical in form to the geostrophic balance conditions applied by Hinkelmann (1951). To obtain better initial balance we turn to second-order constraints (Kasahara, 1982). Rewriting (2.6) by using the definitions in (2.7), we get

$$\left.\begin{aligned}\tilde{u}_t + ik\bar{U}\tilde{u} + a = 0\\ \tilde{v}_t + ik\bar{U}\tilde{v} + b = 0\\ \tilde{h}_t + ik\bar{U}\tilde{h} - f\bar{U}\tilde{v}/g + c = 0\end{aligned}\right\}. \quad (2.9)$$

Therefore, $\tilde{u}_{tt}$, $\tilde{v}_{tt}$ and $\tilde{h}_{tt}$ are of order unity if and only if a_t, b_t and c_t are of order unity. Differentiating (2.7) with respect to time yields

$$\left.\begin{aligned}\epsilon a_t = igk\tilde{h}_t - f\tilde{v}_t\\ \epsilon b_t = f\tilde{u}_t\\ \epsilon^2 c_t = ik\bar{h}\tilde{u}_t\end{aligned}\right\}. \quad (2.10)$$

Again we assume $a_t = b_t = c_t = 0$. Obtaining the first-order time derivatives from (2.6), we find that (2.10) reduces to a simple coupled system of simultaneous equations for $(\tilde{u}/\tilde{h})$ and $(\tilde{v}/\tilde{h})$. In matrix form, (2.10) can be written as

$$\begin{bmatrix}(\epsilon^{-2}gk^2\bar{h}/f + \epsilon^{-1}f) & 2i\bar{U}k\\ ik\bar{U} & -\epsilon^{-1}f\end{bmatrix}\begin{bmatrix}\tilde{u}/\tilde{h}\\ \tilde{v}/\tilde{h}\end{bmatrix} = \begin{bmatrix}-gk^2\bar{U}/f\\ -\epsilon^{-1}igk\end{bmatrix}, \quad (2.11)$$

leading to the following solutions

$$\left.\begin{aligned}(\tilde{u}/\tilde{h}) = \epsilon^2 gk^2\bar{U}/[(k^2g\bar{h} + \epsilon f^2 - 2\epsilon^3k^2\bar{U}^2]\\ (\tilde{v}/\tilde{h}) = (igk/f)[1 + \epsilon^3k^2\bar{U}^2/(k^2g\bar{h} + \epsilon f^2 - 2\epsilon^3k^2\bar{U}^2)]\end{aligned}\right\}. \quad (2.12)$$

Neglecting $O(\epsilon^3)$ terms in the denominator of (2.12) and then setting $\epsilon = 1$ to unscale the remaining terms leads to constraints identical to the ones derived by Philips (1960) through application of quasi-geostrophic considerations. Next, we turn to the balanced conditions based on NMI. The derivation is given in appendix A and here we simply state the results as follows:

$$\left.\begin{aligned}(\tilde{u}/\tilde{h}) = gk^2\bar{U}/(k^2g\bar{h} + f^2 - 2k^2\bar{U}^2)\\ (\tilde{v}/\tilde{h}) = (igk/f)(1 + k^2\bar{U}^2/[k^2g\bar{h} + f^2 - 2\bar{U}^2k^2)]\end{aligned}\right\}, \quad (2.13)$$

which is identical to the unscaled BDI constraints in (2.12) except for the scaling parameter ϵ. In section 3 we shall seek solutions of the prognostic system (2.1) and examine the impact of applying a hierarchy of initial conditions, including the BDI/NMI constraints given by (2.12)/(2.13).

In subsequent analysis it is instructive to note that the harmonic dependency assumed in (2.2) implies that $\tilde{u}/\tilde{h}$ and $\tilde{v}/\tilde{h}$ are proportional to divergence and vorticity, respectively. To obtain analytical solutions of (2.1) we follow Hinklemann (1951) and therefore assume that

$$\left.\begin{aligned}u = \frac{gk}{f}h_0\sum_{n=1}^{3}A_n e^{ik(x-\hat{C}_n t)}\\ v = \frac{igk}{f}h_0\sum_{n=1}^{3}B_n e^{ik(x-\hat{C}_n t)}\\ h = h_0\sum_{n=1}^{3}C_n e^{ik(x-\hat{C}_n t)}\end{aligned}\right\}, \quad (2.14)$$

where h_0 is the amplitude of h; and A_n, B_n and C_n depend purely on the initial values of u and v. We assert

$$\sum_{n=1}^{3}C_n = 1.$$

The $\hat{C}_n$ is the phase velocity and represents the eigenvalue of the problem. For details regarding the computation of these quantites we refer the reader to Hinkelmann (1951). Concerning the computations, it suffices to consider only the real part of (2.14) at a single coordinate point $x = 0$. In this case, according to (2.2) the variables u, v and h are equivalent to the tilde quantities $\tilde{u}$, $\tilde{v}$ and $\tilde{h}$.

We consider three different types of initial conditions. The first case corresponds to an imbalanced state where the vorticity $(\tilde{v})$ is geostrophic and given by (2.8). The divergence, $(\tilde{u})$ is assigned an arbitrary but realistic value of $(0.14)|\tilde{v}_g|$. Here $|\tilde{v}_g|\,(=gkh_0/f)$ is of O(10 m s^{-1}) and corresponds to the magnitude of the geostrophic speed in (2.8). The second case corresponds to geostrophic conditions (2.8), in which case the vorticity is identical to the first case but the divergence vanishes initially. Lastly, the third set of initial conditions are determined by BDI (2.12) or NMI (2.13). Again the vorticity is geostrophic and therefore the same as the first two cases, but the divergence has a different value.

The model constants are $\bar{U} = 30$ m s^{-1}, $\bar{h} = 10^4$ m, $g = 9.8$ m s^{-2}, $f = 10^{-4}$ s^{-1}, the wavelength $L = 3 \times 10^6$ m, and, as usual, $k = 2\pi/L$. We evaluate (2.14) at intervals of 300 s.

For purposes of interpreting the results in Figs. 1a–1c, the height is normalized by h_0, which is its amplitude initially and is representative of typical synoptic motion in middle latitudes. Therefore, h/h_0 is of O(1) for this type of motion. The time evolution of the height, vorticity and divergence, which arise from an unbalanced initial state, is dominated by the presence of high-frequency gravitational oscillations. Application of the first-order constraints of the BDI, which in this case is equivalent to geostrophic balance, results in some improvement over the unbalanced case. In particular, the height amplitude of the gravitational modes is reduced by one order of magnitude. The high-frequency oscillations in the vorticity are practically eliminated. However, the divergence of the gravitational modes still persists and is the same order of magnitude as the one associated with the meteorologically significant Rossby mode. The remaining high frequency oscillations in the height and divergence, which geostrophic balancing fails to remove, are virtually eliminated by the application of the BDI or NMI.

3. The barotropic model

We use the global barotropic model described by Takacs and Balgovind (1983). The effect of orographic forcing is explicitly included in the model. The equations of the model are

$$\frac{\partial u}{\partial t}+\frac{u}{a\cos\phi}\frac{\partial u}{\partial \lambda}+\frac{v}{a}\frac{\partial u}{\partial \phi}-\frac{uv\tan\phi}{a} - fv+\frac{g}{a\cos\phi}\frac{\partial h}{\partial \lambda}=0, \quad (3.1)$$

$$\frac{\partial v}{\partial t}+\frac{u}{a\cos\phi}\frac{\partial v}{\partial \lambda}+\frac{v}{a}\frac{\partial v}{\partial \phi}+\frac{uu\tan\phi}{a}+fu+\frac{g}{a}\frac{\partial h}{\partial \phi}=0, \quad (3.2)$$

$$\frac{\partial h}{\partial t}+\frac{1}{a\cos\phi}\frac{\partial}{\partial \lambda}(uh)+\frac{\partial}{\partial \phi}(vh\cos\phi) + s\delta-\frac{u}{a\cos\phi}\frac{\partial H}{\partial \lambda}+\frac{v}{a}\frac{\partial H}{\partial \phi}=0 \quad (3.3)$$

where h is the deviation of height from the mean h_0 (=9.2 km), u and v are the zonal and meridional wind components, respectively, δ is the divergence, f the Coriolis parameter, H the height of orography, and s is $(h_0 - H)$. Conventional notation is used for longitude (λ) and latitude (ϕ). The time-differencing scheme is Matsuno or leap-frog with a time step of 450 s. We use horizontal resolution of 5° longitude by 4° latitude, and the domain is global. Apart from the inclusion of orography, the present version of the model is identical to the one described by Takacs and Balgovind (1983).

4. Initialization schemes

a. *The bounded-derivative initialization (BDI) method*

We adopt the BDI approach proposed by Browning et al. (1980). In spherical coordinates the scaled balance relationships are

$$\delta=(1/as\cos\phi)\left[u\frac{\partial H}{\partial \lambda}+v\cos\phi\frac{\partial H}{\partial \phi}\right], \quad (4.1)$$

$$g\nabla^2 h-(g/a^2 s\cos^2\phi)\left[\frac{\partial h}{\partial \lambda}\frac{\partial H}{\partial \lambda}+\cos^2\phi\frac{\partial h}{\partial \phi}\frac{\partial H}{\partial \phi}\right] =f\zeta-\beta u+\frac{2}{a^2\cos\phi}\left[\frac{\partial u}{\partial \lambda}\frac{\partial v}{\partial \phi}-\frac{\partial u}{\partial \phi}\frac{\partial v}{\partial \lambda}\right]-\frac{u}{a\cos\phi}\frac{\partial \delta}{\partial \lambda} -\frac{v}{a}\frac{\partial \delta}{\partial \phi}-\delta^2-\frac{1}{a^2\cos\phi}\frac{\partial}{\partial \phi}(u^2+v^2)\sin\phi+\frac{1}{sa\cos\phi} \times\left[\frac{u}{a\cos\phi}\frac{\partial u}{\partial \lambda}+\frac{v}{a}\frac{\partial u}{\partial \phi}-\frac{uv\tan\phi}{a}-fv\right]\frac{\partial H}{\partial \lambda}+\frac{1}{sa} \times\left[\frac{u}{a\cos\phi}\frac{\partial v}{\partial \lambda}+\frac{v}{a}\frac{\partial v}{\partial \phi}+\frac{uu\tan\phi}{a}+fu\right]\frac{\partial H}{\partial \phi}=0, \quad (4.2)$$

where $\epsilon = O(10^{-1})$. The equations are similar to the ones used by Browning et al. (1980) except for the additional terms, which arise from considerations of spherical geometry.

To determine the balanced state using (4.1) and (4.2), we assume that the observations consist only of the rotational wind field, which is calculated from the vorticity of the original field. The divergence is determined by using (4.1), from which we compute the irrotational wind. The total wind vector is obtained by summing the rotational and divergent wind components. The derivation of (4.1) and (4.2) and the numerical algorithm we adopted to solve them are given in appendix B.

b. *Normal-mode initialization (NMI) method*

In general we adopt the standard method suggested by Machenhauer (1977). More specifically, we follow the iterative procedure described by Williamson and Temperton (1981). The normal-mode projector (Bloom, 1983) applied here was developed for the GLA fourth-order GCM. Since the GLA GCM has the same horizontal finite difference discretization as the present model, we adopted the external mode projector with an equivalent depth of 9.2 km to design our NMI scheme. A reasonable balance was achieved in five Machenhauer iterations, leading to a reduction of about four orders of magnitude in the total balance, which is computed in the usual way and thus defined by

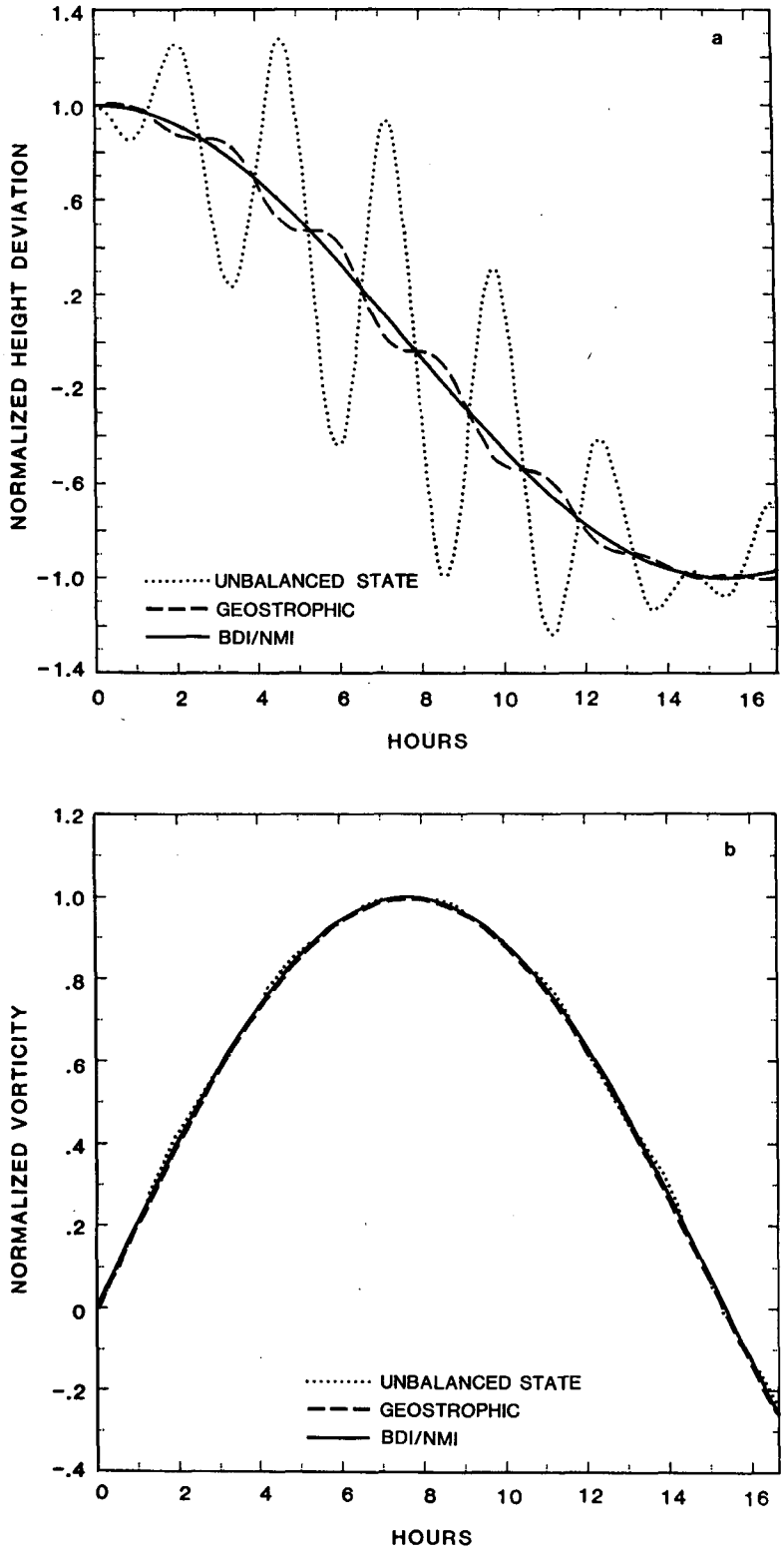

FIG. 1. Time evolution of (a) normalized height (h/h_0) for the linear model, (b) normalized vorticity (V/V_g), and (c) normalized divergence ($U/|V_g|$). The horizontal axis is time in hours.

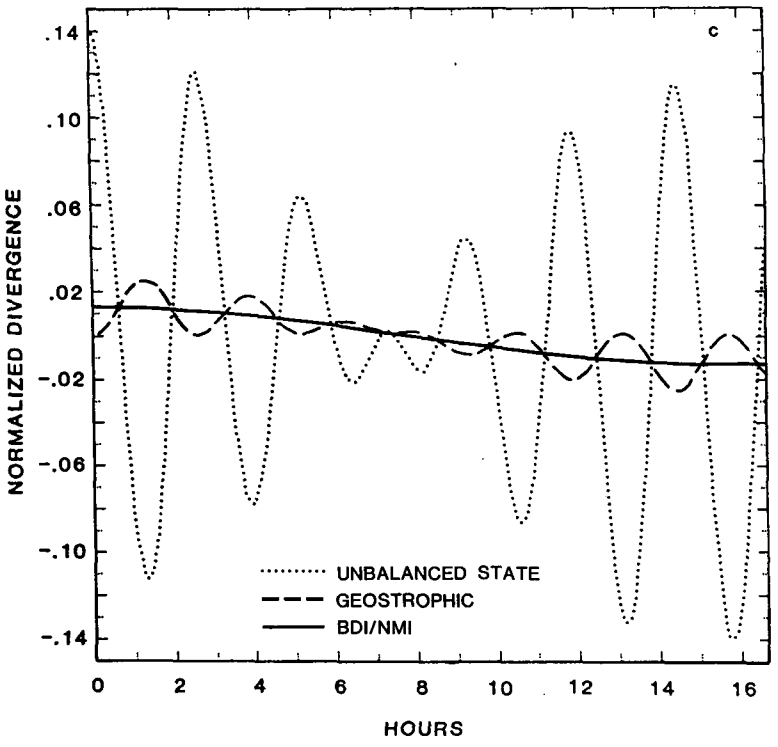

FIG. 1. (*Continued*)

$$\mathrm{BAL} = \sum_m \sum_{l \in G} \left(\frac{\partial c}{\partial t}\right)\left(\frac{\partial c}{\partial t}\right)^*, \qquad (4.3)$$

where c = normal mode coefficient, m = zonal wavenumber, and l = latitudinal indices for the gravity (G) manifold-mode coefficients; BAL is thus the sum of squares of time tendencies of gravity coefficients.

Perhaps we should mention that balanced data based on NMI are constructed by using all the basic prognostic variables of the unbalanced state, namely, u, v and h. In constrast, the BDI used only vorticity to obtain a balanced initial state. We shall compare the initial balanced states of BDI and NMI and their corresponding time evolutions at selected grid points to examine if there is any significant difference in the information that is retained after initialization.

The initial data for our initialization experiments consist of global fields of wind and geopotential heights at 300 mb. They are real data of 0000 GMT 9 January 1979 and were interpolated from the adjacent sigma (σ) levels of the GLA GCM.

5. Discussion of results for the global barotropic model

During subsequent discussions we shall confine ourselves to a limited region in order to permit a more concise comparison. We choose the Asiatic area bounded by latitudes 2°S and 62°N, 60° and 120°E. This window has a number of interesting features. First, the orography (Fig. 2) is very high, which presents an interesting case to examine the nature of adjustment between mass and momentum using different initialization methods. Also, we shall compare the impact of BDI and NMI in the presence of an analysis problem concentrated over this region.

All of the numerical experiments are performed with the Matsuno time-differencing scheme except for one experiment (UBL), which will be described later. We begin the comparison with the height fields for the unbalanced data (UBD), BDI and NMI in Figs. 3a, b, c, respectively. The initialized fields for BDI and NMI are smoother than the unbalanced state; they are also in close agreement. The most noticeable impact of initialization is the suppression of the intense high centered at about 30°N, 90°E, hereafter referred to as the "China high." This feature is a result of the well-known computational problem of interpolating height data between sigma and pressure vertical coordinates. This problem is frequently encountered in most data objective analysis schemes, and clearly, the GLA scheme, which was used to obtain the initial data, is no exception to this shortcoming (Halem et al., 1982). Usually, this problem is most severe in the vicinity of steep slope mountains, but it may occur at other places as well (Gary, 1973). In the present case, the Himalaya mountains are the main sources of the problem. Therefore, one of our objectives is to examine the impact of BDI and NMI over this region with a severe systematic analysis problem.

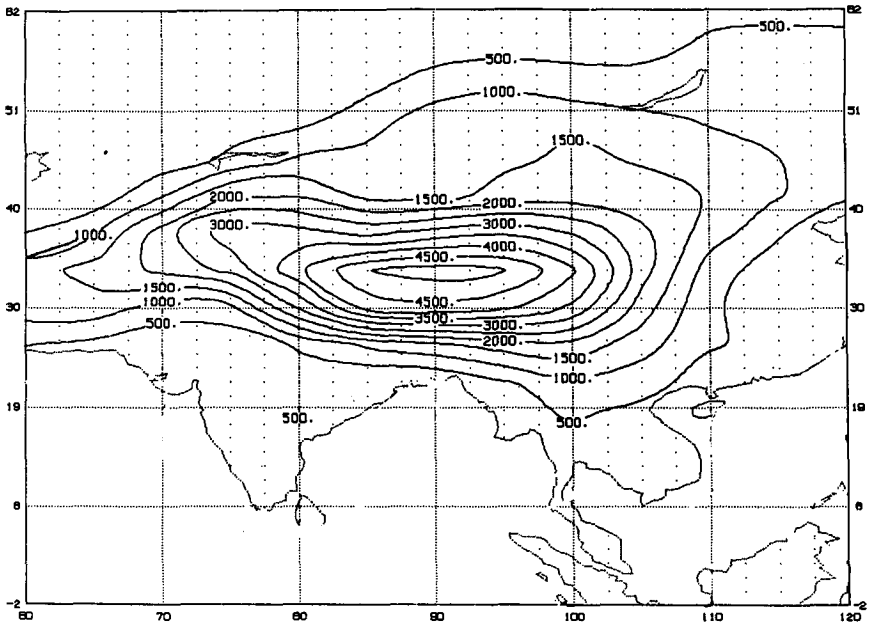

FIG. 2. Orography (m).

It is clear from the comparison of the height field (Fig. 3a) and the vorticity field (Fig. 4a) that the China high is not in quasi-geostrophic balance. Therefore, its absence in the initial state balanced by BDI is not surprising since this method makes use of the vorticity to construct initial conditions.

The results of NMI can be interpreted by first noting that the changes made in the uninitialized state tend to be dictated by the quasi-geostrophic adjustment process. Previous studies (for instance, Williamson and Kasahara, 1971) have demonstrated that for large equivalent depths, such as the one employed in the present study, mass adjusts toward the winds for "short" scale motions. Conversely, at long scales the wind tends to adjust toward mass. In a recent study, Kalnay et al. (1986) discuss the relative importance of

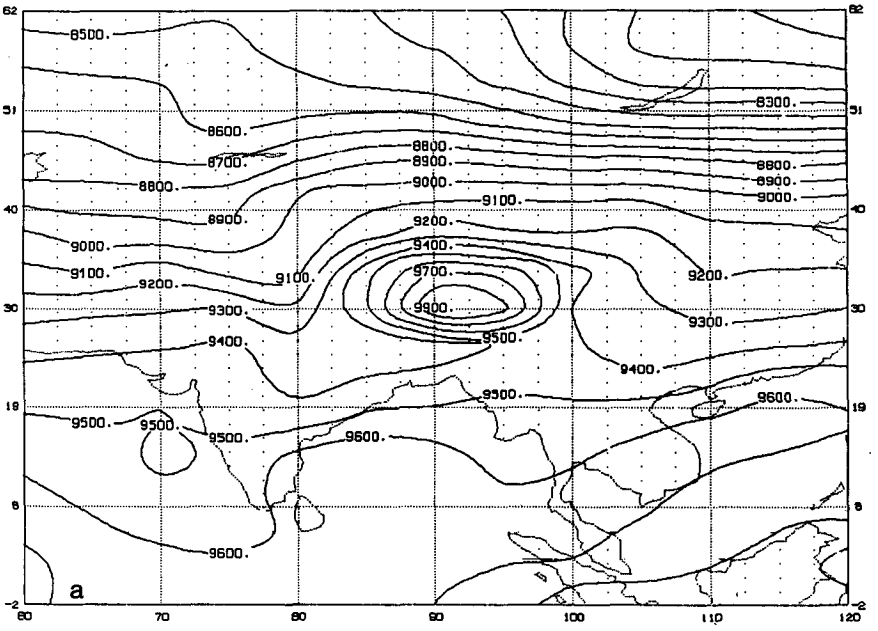

FIG. 3. Heights (m) of the free surface: (a) UBD initial state, (b) BDI initial state, and (c) NMI initial state.

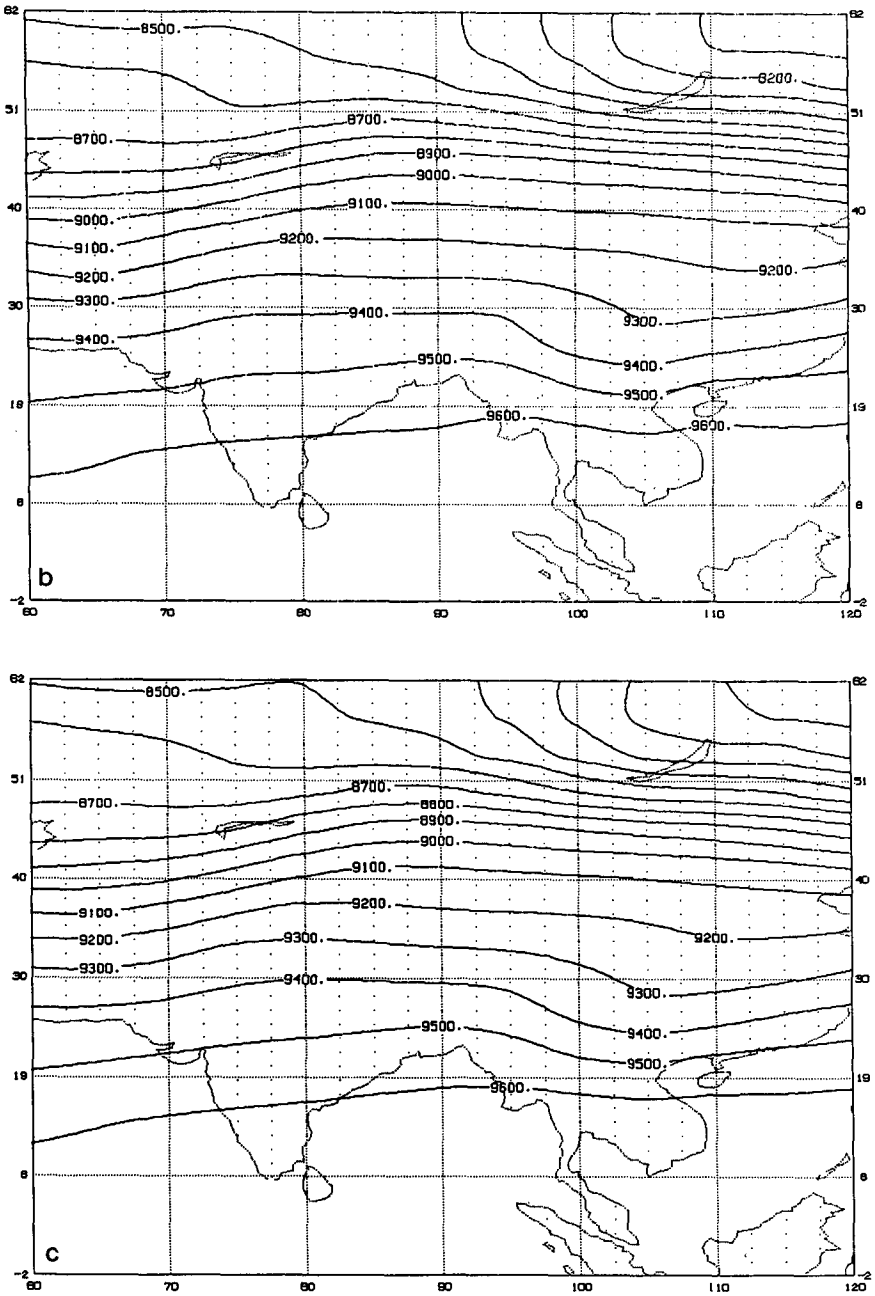

FIG. 3. (*Continued*)

mass and wind data in numerical weather prediction. Using theoretical arguments based on the conservation of potential vorticity, they point out that the typical scale separating short and long scales for slow (Rossby) modes is about 20 000 km for the external mode. Therefore, with the exception of wavenumber 1 and 2, the remaining wavelengths are of short scale, indicating that the China high mass perturbation over the Himalayas, in the unbalanced initial data, is of short scale as well. Consequently, it is clear that as a result of applying NMI, this feature cannot survive the adjustment process since the mass tends to adjust toward the wind field at such scales. If we want to retain the China high, then its projection on the slow manifold must be enhanced, possibly by applying a local geostrophic wind correction that is consistent with the mass perturbation. In fact, this is the basic rationale behind the application of the geostrophic wind correction normally employed in four-dimensional objective data analysis to avoid rejection of information which often

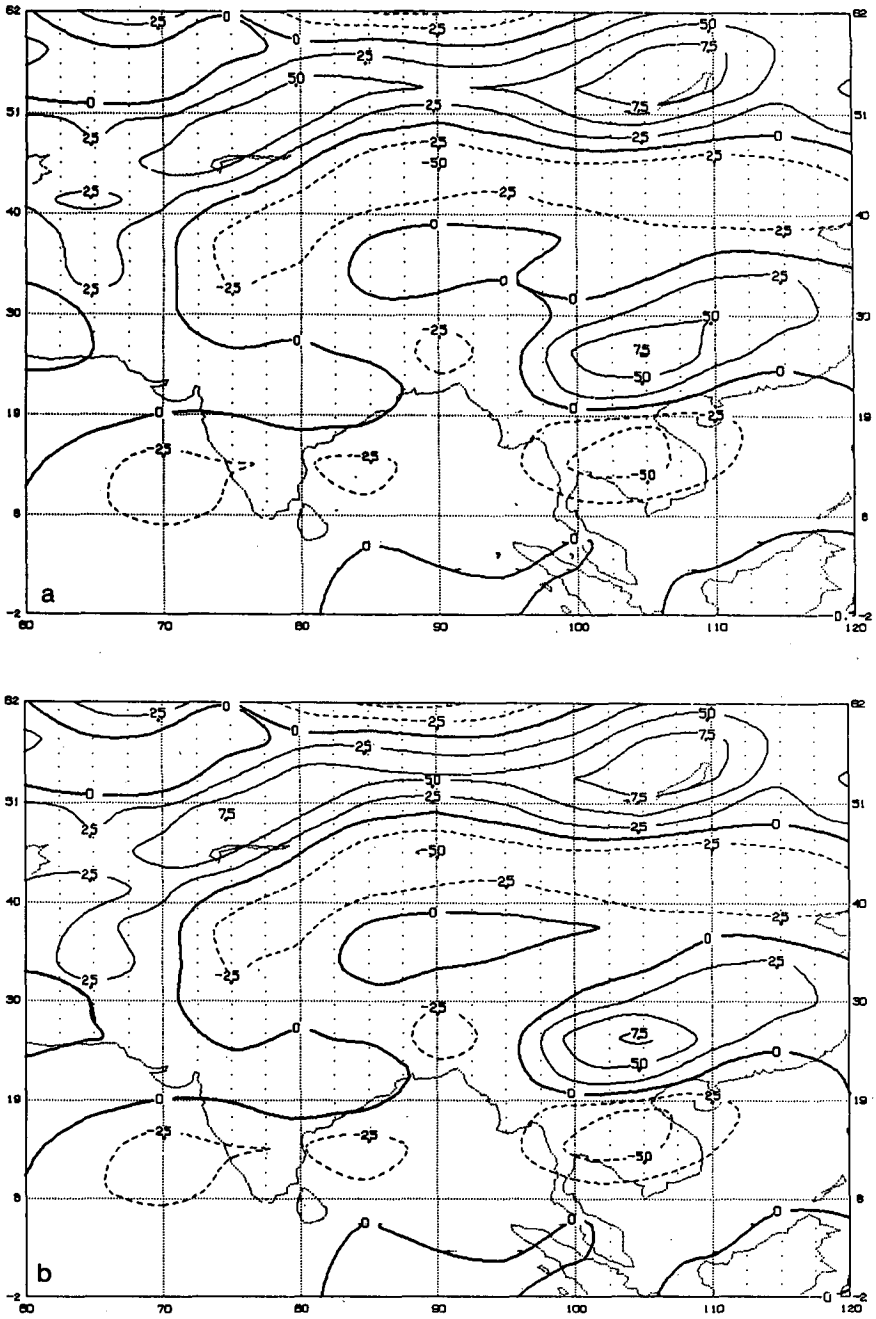

FIG. 4. Vorticity (10^{-5} s^{-1}): (a) BDI/UBD initial state, (b) NMI, (c) vorticity (10^{-6} s^{-1}); BDI/UBD minus NMI. Contour interval is 2.5 × 10^{-5} s^{-1} in (a) and (b), and 10^{-7} s^{-1} in (c).

results from direct assimilation of mass data (Kistler and McPherson, 1975). A more rigorous approach, however, would entail application of constrained NMI (Daley, 1979) by assigning large confidence weights to the relevant variable in the vicinity of trusted observations.

Regarding the motion field, it suffices to consider only the divergence and vorticity. Figure 4a displays the vorticity field for the BDI that is identical to UBD. The corresponding field for NMI is presented in Fig. 4b. The close similarity to UBD/BDI is undisputable. To some extent this justifies the approach in the BDI that does not allow adjustment in the rotational motion during the initialization process. Despite the excellent agreement, a small difference exists between the two fields. In Fig. 4c we show the difference BDM(UBD)

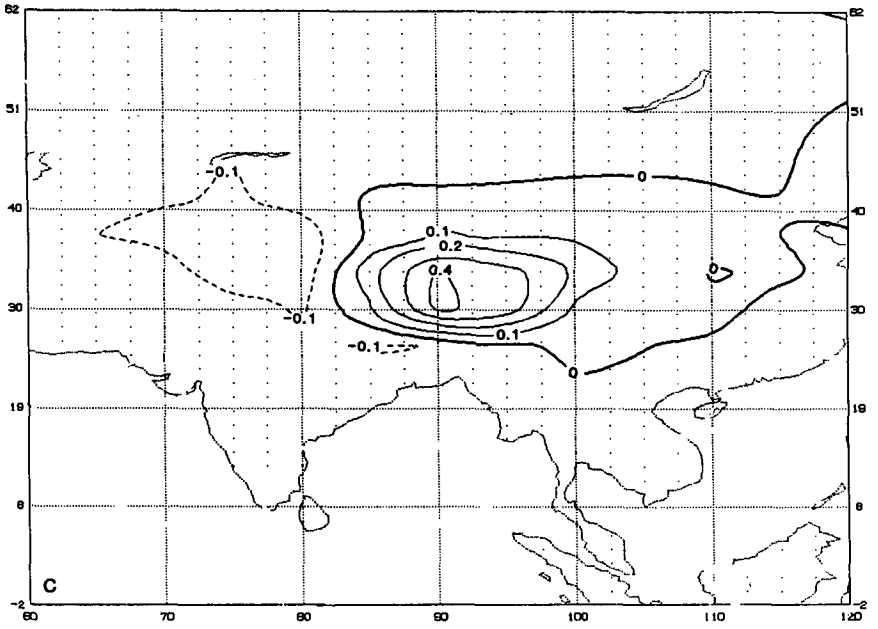

FIG. 4. (*Continued*)

minus NMI. The difference field is typically two orders of magnitude weaker than the actual fields from which it is derived. The most significant feature is the weak vorticity dipole. It is either due to the China high or is a response of initialization to the steep orography in the area. However, the latter possibility was ruled out by performing additional experiments of NMI in which mountains are removed (results not displayed). The dipole vortex persists, which suggests that it is a remnant of the China high. This result is consistent with Puri (1981). Puri showed that directly inserted data with no correction in the wind field is largely projected to the fast manifold. However, a small proportion is also projected to the slow manifold. Unlike the NMI, the BDI cannot retain any proportion of the China high since, in addition to reasons cited earlier, the vorticity is not allowed to change. To some extent this can be argued to imply that the BDI suffers from slight loss of information about the slow manifold contained in the height field. Perhaps this problem can be overcome by designing a BDI scheme that employs height data rather than vorticity, but this question is not pursued any further in this investigation. In any case the actual difference between the information retained by BDI and NMI is insignificant even under the extreme conditions prevailing under the present considerations.

The divergence fields corresponding to the UBD, BDI and NMI are displayed in Figs. 5a, b, c. The unbalanced divergence is completely replaced by new balanced divergence, which is similar for both BDI and NMI. After initialization the typical intensity drops by a factor of 2 or 3 in comparison to the divergence of the uninitialized initial state. As expected, the balanced divergence is centered around regions of highest orography. Similar patterns were found by Semazzi (1985). Typically, divergence prevails over the windward slopes while convergence resides over the leeward slopes of mountains.

The results of each initialization experiment were used as initial data for a 24 h forecast. At intervals of 1 h the values of the height field at two grid points were written to a "grid point history file." The two grid points are B (10°S, 20°E) and A (50°S, 90°E). They represent low and midlatitude locations.

To facilitate a more complete comparison, two additional experiments were performed. In one of these experiments (UBL), the leap-frog time-differencing scheme is used instead of the Matsuno scheme, which is adopted for all the other experiments discussed in this paper. This experiment is equivalent to the UBD experiment except for the change in the time-differencing scheme. In the second additional experiment (CBE) the classical balance equation was applied to initialize the flow at $t = 0$. This corresponds to the case when the orography is zero in the BDI constraints (4.1) and (4.2). Figure 6a shows the time evolution of the height corresponding to UBD, UBL, CBE, BDI and NMI at coordinate A. The forecast starting from UBL suffers from considerable contamination by high-frequency oscillations with a dominant period of about 6 h. At this grid point the Matsuno scheme effectively suppresses high-frequency motions by the end of the 24 h, even without applying initialization. However, during the first part of this forecast the amplitudes of the gravitational oscillations are significant and initialization of the flow at $t = 0$ is necessary to suppress

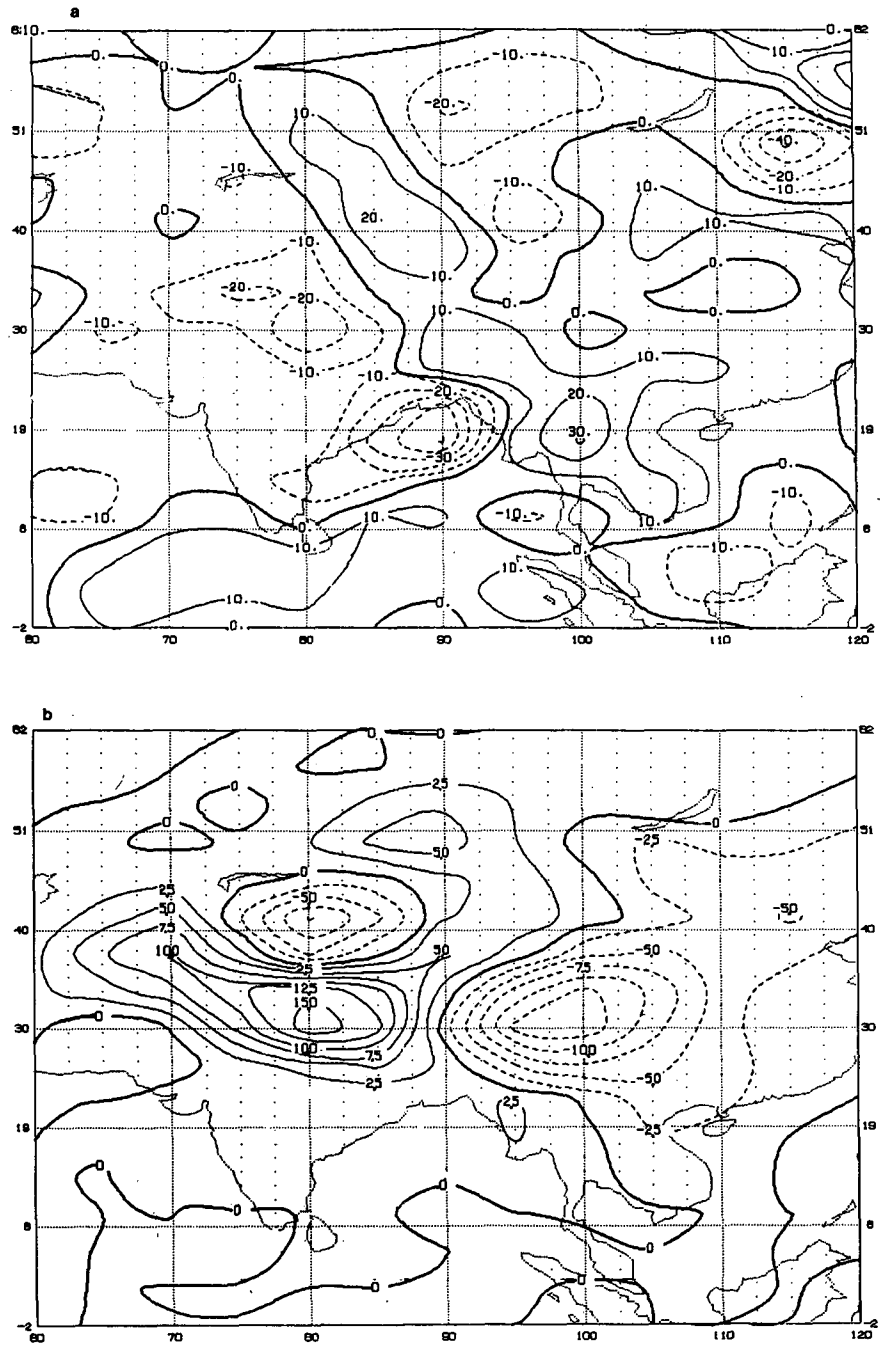

FIG. 5. Divergence (10^{-6} s^{-1}): (a) UBD initial state, (b) BDI initial conditions, and (c) NMI initial conditions. Contour interval is 10^{-6} s^{-1} in (a) and 2.5×10^{-6} s^{-1} in (b) and (c); the maximum contour is (30, 15, 15) $\times 10^{-6}$ s^{-1} in (a), (b), and (c), respectively.

them. Regarding CBE, BDI and NMI, the time evolution is smoother than UBL and UBD. At 24 h of the forecast the impact of the Matsuno scheme in suppressing gravitational motions is comparable to application of BDI or NMI at $t = 0$. The classical balance equation also performs well at this high latitude. The plots for the time evolution for coordinate B are presented in Fig. 6b. Notice that the balance equation performs relatively worse than the NMI and BDI. This is mainly because the balance equation is not capable of handling the gravity waves over regions of low latitude. In this case these waves are excited by the high elevation over equatorial Africa. For the height-field perturbations we note that at low latitudes the amplitudes as-

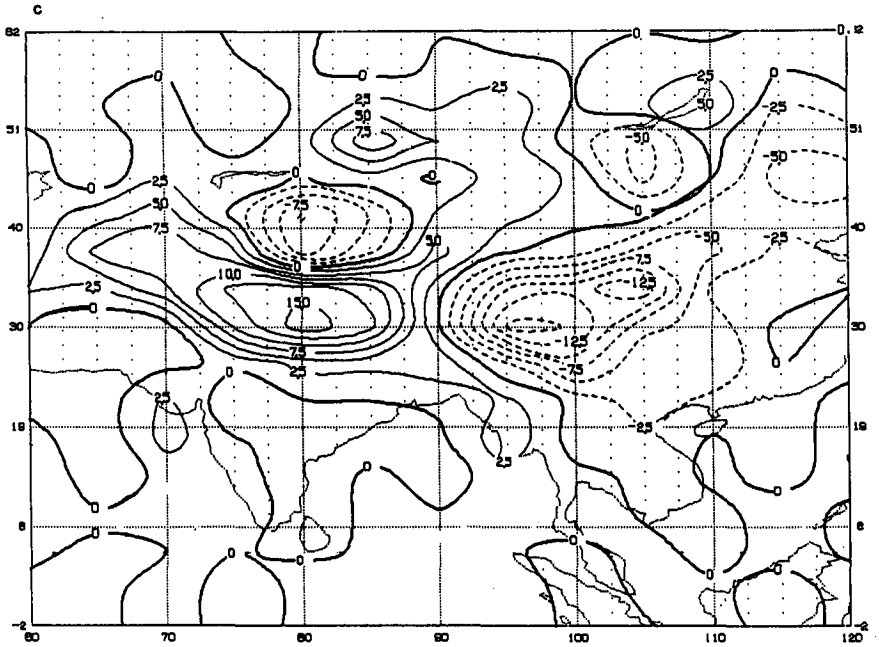

FIG. 5. (*Continued*)

sociated with synoptic waves are typically one order of magnitude smaller than at high latitudes. However, the amplitudes for gravitational motions are similar when we use unbalanced data. This indicates the importance of performing suitable initialization over the low latitude regions of the earth, particularly for purposes of short-range numerical weather predictions.

6. Conclusions

The relationship between the BDI and NMI is examined first, using a simple linear model and then using a nonlinear barotropic model in the presence of realistic initial data.

The calculations based on the linear model indicate that the BDI and NMI are equally effective in suppressing high-frequency oscillations. This is consistent with results of Bijlsma and Hafkenscheid (1986). The initial divergence required to achieve this is of order 10^{-7} s^{-1}, thus in agreement with results of earlier studies.

Concerning the nonlinear model, the results show that despite the difference in the amount of initial data used in either the BDI or the NMI, the balanced states are in close agreement. In particular, both methods eliminate a spurious high present in the unbalanced initial data. If we had confidence in the physical existence of this feature it would be imperative to resort to constrained variational techniques capable of restricting changes in the height field but permitting adjustments in the motion field. Regarding NMI, such an approach was suggested and successfully tested by Daley (1978), but the development of constrained variational BDI is yet to be accomplished. The time evolution of height at selected coordinate points in space during a 24-h period indicates that the unbalanced data are dominated by large-amplitude gravitational oscillations. Both the BDI and the NMI eliminate this noise, and the corresponding forecasts are in close agreement. The results show that the classical balance equation is not as effective as the BDI or NMI methods, particularly in the tropics. Without initialization, the Matsuno time-differencing scheme is incapable of suppressing high-frequency gravitational motions to acceptable levels during the early part of the forecast. However, toward the end of the first day of the forecast its accumulative impact is comparable to the application of BDI or NMI at the initial time. The vorticity of the unbalanced data is only slightly changed by NMI. The divergence field is centered around the regions of high orographic elevation. This distribution is consistent with Semazzi (1985), where divergence prevails over the windward slopes and convergence resides over the leeward slopes of large-scale mountains for both westerly and easterly basic currents.

Lastly, we should note that the present results must be viewed in context of the external mode. The quasi-geostrophic adjustment process, which governs the changes during application of unconstrained initialization, is sensitive to the magnitude of the equivalent depth. Consequently, it is conceivable that the agreement between BDI and NMI in the context to which they have been applied in this study may diminish as smaller equivalent depths are considered, for instance in case of a baroclinic model.

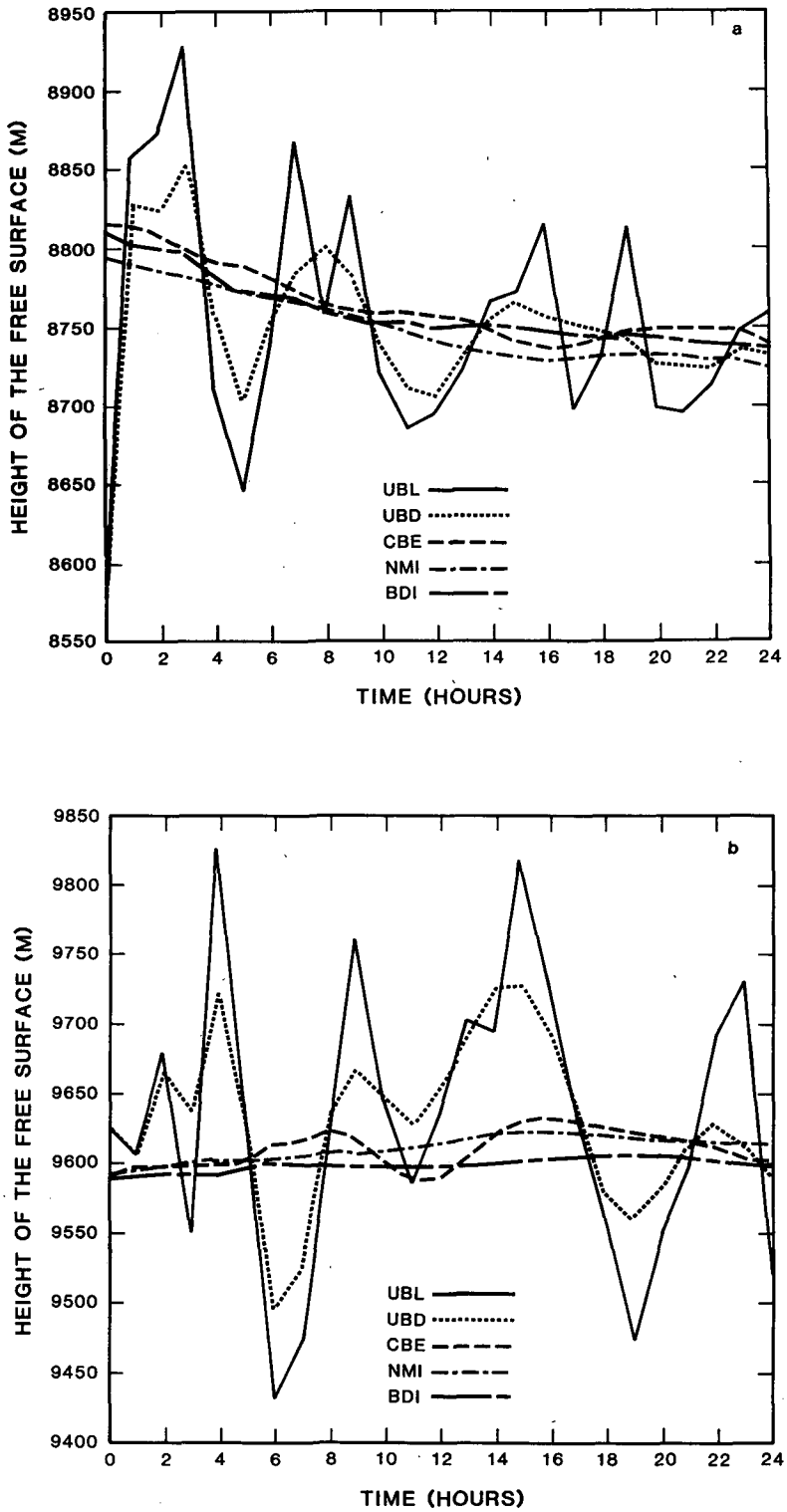

FIG. 6. Time evolution of height at (a) (50°S, 90°E) and (b) (10°S, 20°E). The horizontal axis is time in hours.

Acknowledgments. The authors are very grateful to E. Kalnay for her encouragement during the investigation. The courtesy of S. Bloom for making the normal modes available to the authors is greatly appreciated. Special thanks are due to L. Takacs, who provided his numerical model for use in this study. This research comprised a portion of the doctoral thesis of FHMS. Members of his advisory committee, namely, A. Kasahara, G. C. Asnani and P. Kiangi were very helpful. The support by NCAR and the National Research Council (NRC) to FHMS is greatly appreciated. (NCAR is supported by the National Science Foundation.) Thanks are extended to M. A. Wells and P. H. Marks for efficiently typing the manuscript and to L. Rumburg for drafting the figures.

APPENDIX A

Application of NMI to the Linear Model (2.1)

First, it is convenient to set $\bar{U} = 0$ in (2.1). We get

$$\left.\begin{aligned} u_t - fv + gh_x &= 0 \\ v_t + fu &= 0 \\ h_t + \bar{h}u_x &= 0 \end{aligned}\right\}. \tag{A1}$$

We define

$$\left.\begin{aligned} \hat{u} &= u \\ \hat{v} &= v \\ \hat{h} &= c^{-1}gh \end{aligned}\right\}, \tag{A2}$$

where

$$c = (g\bar{h})^{1/2},$$

so that (A1) may be expressed in the form

$$W_t + LW = 0, \tag{A3}$$

where

$$W = \begin{pmatrix} \hat{u} \\ \hat{v} \\ \hat{h} \end{pmatrix}, \tag{A4}$$

$$L = \begin{pmatrix} 0 & -f & c(\ )_x \\ f & 0 & 0 \\ c(\ )_x & 0 & 0 \end{pmatrix}. \tag{A5}$$

We assume harmonic dependency such that

$$W = H\exp[i(\omega t + kx)], \tag{A6}$$

where ω is the frequency, k the wavenumber, and H the model vector. Substituting (A6) into (A3) results in a cubic equation with roots given by

$$\left.\begin{aligned} \omega_R &= 0 \\ \omega_{\pm G} &= \pm(c^2k^2 + f^2)^{1/2} = \pm\sigma_G \end{aligned}\right\}, \tag{A7}$$

where ω_R is the low frequency of the Rossby mode and $\omega_{\pm G}$ denotes the high frequency of the eastward- and westward-propagating gravity waves. The corresponding eigenvectors are

$$\left.\begin{aligned} H_R &= \sigma_G^{-1}\begin{pmatrix} 0 \\ ikc \\ f \end{pmatrix} \\ H_{\pm G} &= \frac{\sigma_G^{-1}}{\sqrt{2}}\begin{pmatrix} \pm i\sigma_G \\ -f \\ -ikc \end{pmatrix} \end{aligned}\right\}. \tag{A8}$$

Multiplication by $H_{\pm G}^*$, the complex conjugate of $H_{\pm G}$, isolates the gravitational eigenmodes (Kasahara, 1982). Before we make use of this convenient property, we first present (2.3) in the form

$$\begin{bmatrix} \tilde{u} \\ \tilde{v} \\ \tilde{z} \end{bmatrix}_t + \begin{bmatrix} -f\tilde{v} + ick\tilde{z} \\ f\tilde{u} \\ ick\tilde{u} \end{bmatrix} = \begin{bmatrix} -ik\bar{U}\tilde{u} \\ -ik\bar{U}\tilde{v} \\ c^{-1}f\bar{U}\tilde{v} - ik\bar{U}\tilde{z} \end{bmatrix}, \tag{A9}$$

where

$$\tilde{z} = c^{-1}g\tilde{h}, \tag{A10}$$

by defining

$$\left.\begin{aligned} W_{\pm G} &= i\omega_{\pm G}\tilde{u} + ikc\tilde{z} - f\tilde{v} \\ N_{\pm G} &= ik\bar{U}(f\tilde{v} - W_{\pm G}) \end{aligned}\right\} \tag{A11}$$

and then operating $H_{\pm G}^*$ on (A9) yields

$$(W_{\pm G})_t + i\omega_{\pm G}W_{\pm G} = N_{\pm G}. \tag{A12}$$

We treat (A12) as if it is a nonlinear equation with $N_{\pm G}$ representing the nonlinear forcing (Phillips, 1981).

To perform NMI we follow the approach proposed by Machenhauer (1977). In this case we require the time tendency of the gravity modes in (A12) to be zero. This condition, together with the use of (A11), yields

$$W_{\pm G} = \frac{k\bar{U}}{\omega_{\pm G}}f\tilde{v}\left(1 + \frac{k\bar{U}}{\omega_{\pm G}}\right)^{-1}. \tag{A13}$$

We can obtain $\tilde{u}$ and $\tilde{v}$ corresponding to (A13) by using the definition of $W_{\pm G}$ in (A11) and solving the resulting coupled system of equations. This gives

$$\left.\begin{aligned} \frac{\tilde{u}}{\bar{h}} &= \frac{gk^2\bar{U}}{[k^2g\bar{h} + f^2 - 2k^2\bar{U}^2]} \\ \frac{\tilde{v}}{\bar{h}} &= (igk/f)[1 + k^2\bar{U}^2/(k^2g\bar{h} + f^2 - 2\bar{U}^2k^2)] \end{aligned}\right\}. \tag{A14}$$

APPENDIX B

Derivation of the BDI Balance Constraints (4.1) and (4.2)

Recently, Browning et al. (1980) discussed initialization schemes based on BDI for a barotropic model, separately for equatorial and middle latitude β-planes. Their results indicate that the balance constraints based on equatorial considerations are similar but more restrictive than the ones for middle latitudes. A suitable, unified initialization scheme for the entire globe is the one based on the constraints for the low latitudes.

In the present study we consider a global domain. We assume the following characteristic scales for equatorial synoptic motion:

$$\left.\begin{aligned} a\delta\phi \approx a\delta\lambda \sim O(10^6\,\mathrm{m}) \\ u, v \approx O(10\,\mathrm{m\,s^{-1}}) \\ t \approx O(10^5\,\mathrm{s}) \\ h \approx O(10\,\mathrm{m}) \\ s \approx O(10^4\,\mathrm{m}) \\ g \approx O(10\,\mathrm{m\,s^{-2}}) \\ H \approx O(10^3\,\mathrm{m}) \\ a \approx O(10^7\,\mathrm{m}) \\ f \approx O(10^{-5}\,\mathrm{s^{-1}}) \end{aligned}\right\}. \tag{B1}$$

We make allowances for a global domain and assume that $(\tan\phi)$ can be as large as O(10). This simply ensures that this term is not neglected during the scaling process.

Scaling (3.1) and (3.3) using (B1) yields

$$\frac{\partial u}{\partial t}+\frac{u}{a\cos\phi}\frac{\partial u}{\partial\lambda}+\frac{v}{a}\frac{\partial u}{\partial\phi}-\frac{uv\tan\phi}{a}-fv+\frac{g}{a\cos\phi}\frac{\partial h}{\partial\lambda}=0, \tag{B2}$$

$$\frac{\partial v}{\partial t}+\frac{u}{a\cos\phi}\frac{\partial v}{\partial\lambda}+\frac{v}{a}\frac{\partial u}{\partial\phi}+\frac{vu\tan\phi}{a}+fu+\frac{g}{a}\frac{\partial h}{\partial\phi}=0, \tag{B3}$$

$$\frac{\partial h}{\partial t}+\frac{1}{a\cos\phi}\left[\frac{\partial(uh)}{\partial\lambda}+\frac{\partial}{\partial\phi}(vh)\cos\phi\right]+\epsilon^{-3}S\delta - \epsilon^{-2}\left[\frac{u}{a\cos\phi}\frac{\partial H}{\partial\lambda}+\frac{v}{a}\frac{\partial H}{\partial\phi}\right]=0, \tag{B4}$$

where all the variables are nondimensional and are of order unity except the scaling parameter, $\epsilon = O(10^{-1})$.

Following Browning et al. (1980), the first-order time derivatives u_t, v_t and h_t are of order unity if and only if

$$s\delta-\epsilon\left(\frac{u}{a\cos\phi}\frac{\partial H}{\partial\lambda}+\frac{v}{a}\frac{\partial H}{\partial\phi}\right)=\epsilon^3 C, \tag{B5}$$

where C is smooth and of order unity.

To obtain a second constraint, we substitute (B5) into (B4). The result is

$$\frac{\partial h}{\partial t}+\frac{1}{a\cos\phi}\left[\frac{\partial(uh)}{\partial\lambda}+\frac{\partial}{\partial\phi}(vh)\cos\phi\right]+C=0. \tag{B6}$$

Therefore, the second-order time derivatives u_{tt}, v_{tt}, h_{tt} are also of order unity if and only if C_t is of order unity. By differentiating (B5) it is easy to show that the second constraint is given by

$$g\nabla^2 h-(g/a^2 s\cos^2\phi)\left[\frac{\partial u}{\partial\lambda}\frac{\partial H}{\partial\lambda}+\cos^2\phi\frac{\partial h}{\partial\phi}\frac{\partial H}{\partial\phi}\right] =f\zeta-\beta u+\frac{2}{a^2\cos\phi}\left[\frac{\partial u}{\partial\lambda}\frac{\partial v}{\partial\phi}-\frac{\partial u}{\partial\phi}\frac{\partial v}{\partial\lambda}\right]-\frac{u}{a\cos\phi}\frac{\partial\delta}{\partial\lambda} -\frac{v}{a}\frac{\partial\delta}{\partial\phi}-\delta^2-\frac{1}{a^2\cos\phi}\frac{\partial}{\partial\phi}(u^2+v^2)\sin\phi +\frac{\epsilon}{sa\cos\phi}\left[\frac{u}{a\cos\phi}\frac{\partial u}{\partial\lambda}+\frac{v}{a}\frac{\partial u}{\partial\phi}-\frac{uv\tan\phi}{a}-fv\right]\frac{\partial H}{\partial\lambda} +\frac{\epsilon}{sa}\left[\frac{u}{a\cos\phi}\frac{\partial v}{\partial\lambda}+\frac{v}{a}\frac{\partial v}{\partial\phi}+\frac{uu\tan\phi}{a}+fu\right]\frac{\partial H}{\partial\phi}+\epsilon^3 C_t. \tag{B7}$$

The easiest way to satisfy (B5) and (B7) is to neglect terms $O(\epsilon^3)$ and set $\epsilon^3 C = \epsilon^3 C_t = 0$. Finally we set $\epsilon = 1$ to unscale the resulting system of equations and obtain the balance constraints stated in (4.1)–(4.3).

To determine the initial divergence and height fields using (4.1) and (4.2) we adopt the following iterative scheme:

$$\delta^{k+1}=(1/as\cos\phi)\left(u^k\frac{\partial H}{\partial\lambda}+v^k\cos\phi\frac{\partial H}{\partial\phi}\right), \tag{B8}$$

$$g\nabla^2 h^{k+1}-(g/a^2 s\cos^2\phi)\left[\frac{\partial h^{k+1}}{\partial\lambda}\frac{\partial H}{\partial\lambda}+\cos^2\phi\frac{\partial h^{k+1}}{\partial\phi}\frac{\partial H}{\partial\phi}\right] =f\zeta-\beta u^k+\frac{2}{a^2\cos\phi}\left[\frac{\partial u^k}{\partial\lambda}\frac{\partial v^k}{\partial\phi}-\frac{\partial u^k}{\partial\phi}\frac{\partial v^k}{\partial\lambda}\right]-\frac{u^k}{a\cos\phi} \times\frac{\partial\delta^k}{\partial\lambda}-\frac{v^k}{a}\frac{\partial\delta^k}{\partial\phi}-(\delta^k)^2-\frac{1}{a^2\cos\phi}\frac{\partial}{\partial\phi}[(u^k)^2+(v^k)^2]\sin\phi +\frac{1}{sa\cos\phi}\left[\frac{u^k}{a\cos\phi}\frac{\partial u^k}{\partial\lambda}+\frac{v^k}{a}\frac{\partial u^k}{\partial\phi}-\frac{u^k v^k}{a}\tan\phi-fv^k\right] \times\frac{\partial H}{\partial\lambda}+\frac{1}{as}\left[\frac{u^k}{a\cos\phi}\frac{\partial v^k}{\partial\lambda}+\frac{v^k}{a}\frac{\partial v^k}{\partial\phi} +\frac{u^k u^k}{a}\tan\phi+fu^k\right]\frac{\partial H}{\partial\phi}, \tag{B9}$$

where $k = 0, \ldots, K\,(=3)$. For $k = 0$, we assume the motion is comprised of only the rotational components of the original unbalanced initial state, which are computed from the relations

$$\left.\begin{aligned} \nabla^2\psi &= \zeta \\ u_\psi &= -\frac{1}{a}\frac{\partial\psi}{\partial\phi} \\ v_\psi &= \frac{1}{a\cos\phi}\frac{\partial\psi}{\partial\lambda} \end{aligned}\right\}, \tag{B10}$$

where ψ is the streamfunction of the initial unbalanced state and does not change during the iteration process, ζ is the initial vorticity, and u_ψ and v_ψ are the zonal and meridional components of the rotational flow. Once divergence is determined from (B8), the irrotational velocity components are calculated from

$$\left.\begin{aligned} \nabla^2\chi^k &= \delta^k \\ u_\chi{}^k &= \frac{1}{a\cos\phi}\frac{\partial\chi^k}{\partial\lambda} \\ v_\chi{}^k &= \frac{1}{a}\frac{\partial\chi^k}{\partial\phi} \end{aligned}\right\}. \qquad \text{(B11)}$$

The total motion field of the unbalanced state is obtained by summing the irrotational and rotational components. Then, these are substituted into (B9) to compute the balanced height field. To be consistent with other calculations in this investigation the spatial derivatives are performed using fourth-order accuracy.

REFERENCES

Baer, F., 1977: Adjustment of initial conditions required to suppress gravity oscillations in nonlinear flows. *Beitr. Phys. Atmos.*, **50**, 350–366.

Bijlsma, S. J., and L. M. Hafkenscheid, 1986: Initialization of limited area model: A comparison between the nonlinear normal mode and bounded derivative methods. *Mon. Wea. Rev.*, **114**, 1445–1455.

Bloom, S., 1983: Normal modes of the GLAS 4th order model. NASA Research Review 1982, Global Modeling and Simulation Branch. NASA Tech. Memo. 84983, 99–103.

Bourke, W., and J. L. McGregor, 1983: A nonlinear vertical mode initialization scheme for a limited area prediction model. *Mon. Wea. Rev.*, **111**, 2285–2296.

Browning, G., 1982: Initialization of shallow water equations with open boundaries by the bounded derivative method. *Tellus*, **34**, 334–351.

——, A. Kasahara and H. O. Kreiss, 1980: Initialization of the primitive equations by the bounded derivative method. *J. Atmos. Sci.*, **37**, 1424–1436.

Briere, S., 1982: Nonlinear normal mode initialization of a limited area model. *Mon. Wea. Rev.*, **110**, 1166–1186.

Daley, R., 1978: Variational nonlinear normal mode initialization. *Tellus*, **30**, 201–218.

——, 1981: Normal mode initialization. *Rev. Geophys. Space Phys.*, **3**, 350–468.

Gary, J. M., 1973: Estimate of truncation error in transformed coordinate, primitive equation atmospheric model. *J. Atmos. Sci.*, **30**, 223–233.

Halem, M., E. Kalnay-Rivas, W. E. Baker and R. Atlas, 1982: An assessment of the FGGE satellite observing system during SOP-1. *Bull. Amer. Meteor. Soc.*, **63**, 407–426.

Hinkelmann, K., 1951: Der mechanisms des meteorologischen Larmes. *Tellus*, **3**, 350–468.

Kalnay, E., J. C. Jusem and J. Pfaendtner, 1986: The relative importance of mass and wind in the present observing system. *Nat. Conf. on Scientific Results of the GARP Global Experiment*, Miami, 268 pp.

Kasahara, K., 1982: Nonlinear normal mode initialization and the bounded derivative method. *Rev. Geophys. Space Phys.*, **20**, 385–397.

Kistler, R., and R. McPherson, 1975: On the use of local wind correction technique in four-dimensional data assimilation. *Mon. Wea. Rev.*, **103**, 445–449.

Kitade, T., 1983: Nonlinear normal mode initialization with physics. *Mon. Wea. Rev.*, **111**, 2194–2213.

Kreiss, H. O., 1979: Problems with different time scales for ordinary differential equations. *Siam J. Num. Anal.*, **16**, 980–998.

——, 1980: Problems with different time scales for partial differential equations. *Commun. Pure Appl. Math.*, **33**, 399–437.

Machenhauer, B., 1977: On the dynamics of gravity oscillations in a shallow water model, with application to normal mode initialization. *Beitr. Phys. Atmos.*, **50**, 253–271.

Phillips, N. A., 1960: On the problems of initial data for primitive equations. *Tellus*, **12**, 121–126.

——, 1981: Treatment of normal and abnormal modes. *Mon. Wea. Rev.*, **109**, 1117–1119.

Puri, K., 1981: Local geostrophic wind correction in the assimilation of height data and its relationship to the slow manifold. *Mon. Wea. Rev.*, **109**, 52–55.

——, 1985: Sensitivity of low latitude velocity potential field in a numerical weather prediction model to initial conditions, initialization and physical processes. *Mon. Wea. Rev.*, **113**, 449–466.

Rasch, P. J., 1985: Developments in normal mode initialization. Part II. A new method and its comparison with currently used schemes. *Mon. Wea. Rev.*, **113**, 1753–1770.

Semazzi, F. H. M., 1985: On the investigation of the equatorial orographic dynamic mechanism. *J. Atmos. Sci.*, **42**, 78–83.

Takacs, L. L., and R. C. Balgovind, 1983: High latitude filtering in grid point models. *Mon. Wea. Rev.*, **111**, 2005–2015.

Tribbia, J., 1984: A simple scheme for higher order nonlinear normal mode initialization. *Mon. Wea. Rev.*, **112**, 278–284.

Williamson, D. L., and A. Kasahara, 1971: Adaptation of meteorological variables forced by updating. *J. Atmos. Sci.*, **28**, 1313–1324.

——, and C. Temperton, 1981: Normal mode initialization for a multilevel grid point model. II, Nonlinear aspects. *Mon. Wea. Rev.*, **109**, 744–757.